3346 *Chem. Mater.* **2009,** *21,* 3346–3355
DOI:10.1021/cm9012969

CHEMISTRY OF MATERIALS
Article

Selective Gas Adsorption in One-Dimensional, Flexible Cu^{II} Coordination Polymers with Polar Units

Shin-ichiro Noro,*[,†] Daisuke Tanaka,[‡] Hirotoshi Sakamoto,[‡] Satoru Shimomura,[‡] Susumu Kitagawa,[‡,∥] Sadamu Takeda,[$] Kazuhiro Uemura,[⊥] Hidetoshi Kita,[⊥] Tomoyuki Akutagawa,[†] and Takayoshi Nakamura*[,†]

[†]*Research Institute for Electronic Science, Hokkaido University, Sapporo 001-0020, Japan,* [‡]*Department of Synthetic Chemistry and Biological Chemistry, Graduate School of Engineering, Kyoto University, Katsura, Nishikyo-ku, Kyoto 615-8510, Japan,* [∥]*Institute for Integrated Cell-Material Science (iCeMS), Kyoto University, Yoshida, Sakyo-ku, Kyoto 606-8501, Japan,* [$]*Department of Chemistry, Faculty of Science, Hokkaido University, Sapporo 060-0812, Japan, and* [⊥]*Environmental Science and Engineering, Graduate School of Science and Engineering, Yamaguchi University, Tokiwadai 2-16-1, Ube-shi, Yamaguchi 755-8611, Japan*

Received May 11, 2009

Introducing polar $Cu-PF_6$ parts into a coordination framework will open new routes in the fabrication of high-performance and/or novel functional porous materials. We have designed and synthesized the one-dimensional Cu^{II} coordination polymer $[Cu(PF_6)_2(bpetha)_2]_n$ (**1**), with weak and flexible $Cu-PF_6$ parts. **1** shows the property of highly selective adsorption for CO_2 and C_2H_2 gases, which interact with the F atoms of the polar $Cu-PF_6$ parts. Crystallographic characterization of $[Cu(PF_6)_2(4\text{-mepy})_4]$ (**2**) with a basic $[Cu(PF_6)_2(pyridine)_4]$ structure indicates that **2** forms weak $Cu-PF_6$ bonds at its axial sites and the polarity of the surface in **2** is higher than that in α-$[Ni(NCS)_2(4\text{-mepy})_4]$. The axial ligand-exchanged frameworks, $[Cu(PF_6)_{1.4}(BF_4)_{0.6}(bpetha)_2]_n$ (**3**) and $\{[Cu(bpetha)_2(DMF)_2]\cdot 2PF_6\}_n$ (**4**), enable us to control the onset pressure and maximum adsorption amount for targeted CO_2 gases, showing the first case of finely controlled adsorption properties using one-dimensional porous coordination polymers.

Introduction

Porous coordination polymers (PCPs) are promising solids for molecular storage/separation and heterogeneous catalysis because they possess designable frameworks (size, shape, and surface potential) with high regularity, porosity, and flexibility.[1] These characteristics differ from those of conventional porous materials, such as zeolites, activated carbons, and organic supramolecular hosts. In recent years, many PCPs with three-dimensional frameworks that provide new sizes, shapes, and varied internal surface environments have been synthesized. Because of their permanent porosity and high surface area, they are good candidates for developing high-performance adsorbents,[1o,2] catalysts,[3] and reaction vessels.[4] In contrast, some PCPs show a stepwise adsorption caused by a guest-induced framework transition, which

*Corresponding author. E-mail: noro@es.hokudai.ac.jp (S-i.N.); tnaka@es.hokudai.ac.jp (T.N.).

(1) (a) Kitagawa, S.; Kitaura, R.; Noro, S. *Angew. Chem., Int. Ed.* **2004**, *43*, 2334. (b) Yaghi, O. M.; O'Keeffe, J.; Ockwig, N. W.; Chae, H. K.; Eddaoudi, M.; Kim, J. *Nature* **2003**, *423*, 705. (c) Férey, G. *Chem. Soc. Rev.* **2008**, *37*, 191. (d) Bradshaw, D.; Claridge, J. B.; Cussen, E. J.; Prior, T. J.; Rosseinsky, M. J. *Acc. Chem. Res.* **2005**, *36*, 273. (e) Moulton, B.; Zaworotko, M. J. *Chem. Rev.* **2001**, *101*, 1629. (f) Janiak, C. *Dalton Trans* **2003**, 2781. (g) Kesanli, B.; Lin, W. B. *Coord. Chem. Rev.* **2003**, *246*, 205. (h) Kepert, C. J. *Chem Commun.* **2006**, 695. (i) Kawano, M.; Fujita, M. *Coord. Chem. Rev.* **2007**, *251*, 2592. (j) Chandler, B. D.; Enright, G. D.; Udachin, K. A.; Pawsey, S.; Ripmeester, J. A.; Cramb, D. T.; Shimizu, G. K. H. *Nat. Mater.* **2008**, *7*, 229. (k) Samsonenko, D. G.; Kim, H.; Sun, Y.; Kim, G.-H.; Lee, H.-S.; Kim, K. *Chem. Asian. J.* **2007**, *2*, 484. (l) Bárcia, P. S.; Zapata, F.; Silva, J. A. C.; Rodrigues, A. E.; Chen, B. *J. Phys. Chem. B* **2007**, *111*, 6101. (m) Kaye, S. S.; Long, J. R. *J. Am. Chem. Soc.* **2008**, *130*, 806. (n) Ma, S.; Sun, D.; Simmons, J. M.; Collier, C. D.; Yuan, D.; Zhou, H.-C. *J. Am. Chem. Soc.* **2008**, *130*, 1012–1016. (o) Hermes, S.; Schröter, M.-K.; Schmid, R.; Khodeir, L.; Muhler, M.; Tissler, A.; Fischer, R. W.; Fischer, R. A. *Angew. Chem., Int. Ed.* **2005**, *44*, 6237. (p) Takamizawa, S.; Nakata, E.; Akatsuka, T. *Angew. Chem., Int. Ed.* **2006**, *45*, 2216. (q) Lee, E. Y.; Jang, S. Y.; Suh, M. P. *J. Am. Chem. Soc.* **2005**, *127*, 6374. (r) Kondo, A.; Noguchi, H.; Carlucci, L.; Proserpio, D. M.; Ciani, G.; Kajiro, H.; Ohba, T.; Kanoh, H.; Kaneko, K. *J. Am. Chem. Soc.* **2007**, *129*, 12363. (s) Song, Y.-F.; Cronin, L. *Angew. Chem., Int. Ed.* **2008**, *47*, 4635. (t) Farha, O. K.; Spokoyny, A. M.; Mulfort, K. L.; Hawthorne, M. F.; Mirkin, C. A.; Hupp, J. T. *J. Am. Chem. Soc.* **2007**, *129*, 12680. (u) Xiao, B.; Wheatley, P. S.; Zhao, X. B.; Fletcher, A. J.; Fox, S.; Rossi, A. G.; Megson, I. L.; Bordiga, S.; Regli, L.; Thomas, K. M.; Morris, R. E. *J. Am. Chem. Soc.* **2007**, *129*, 1203. (v) Nouar, F.; Eubank, J. F.; Bousquet, T.; Wojtas, L.; Zaworotko, M. J.; Eddaoudi, M. *J. Am. Chem. Soc.* **2008**, *130*, 1833. (w) Tanabe, K. K.; Wang, Z.; Cohen, S. M. *J. Am. Chem. Soc.* **2008**, *130*, 8508. (x) Maji, T. K.; Matsuda, R.; Kitagawa, S. *Nat. Mater.* **2007**, *6*, 142. (y) Noro, S.; Kitagawa, S.; Akutagawa, T.; Nakamura, T. *Prog. Polym. Sci.* **2009**, *34*, 240.

(2) (a) Férey, G.; Mellot-Draznieks, C.; Serre, C.; Millange, F.; Dutour, J.; Surblé, S.; Margiolaki, I. *Science* **2005**, *309*, 2040. (b) Chui, S. S.-Y.; Lo, S. M.-F.; Charmant, J. P. H.; Orpen, A. G.; Williams, I. D. *Science* **1999**, *283*, 1148. (c) Eddaoudi, M.; Kim, J.; Rosi, N.; Vodak, D.; Wachter, J.; O'Keeffe, M.; Yaghi, O. M. *Science* **2002**, *295*, 469. (d) Banerjee, R.; Phan, A.; Wang, B.; Knobler, C.; Furukawa, H.; O'Keeffe, M.; Yaghi, O. M. *Science* **2008**, *319*, 939. (e) Dinc, M.; Long, J. R. *J. Am. Chem. Soc.* **2007**, *129*, 11172. (f) Chun, H.; Dybtsev, D. N.; Kim, H.; Kim, K. *Chem.—Eur. J.* **2005**, *11*, 3521. (g) Hou, L.; Lin, Y.-Y.; Chen, X.-M. *Inorg. Chem.* **2008**, *47*, 1346.

(3) (a) Wu, C.-D.; Hu, A.; Zhang, L.; Lin, W. *J. Am. Chem. Soc.* **2005**, *127*, 8940. (b) Horike, S.; Dinc, M.; Tamaki, K.; Long, J. R. *J. Am. Chem. Soc.* **2008**, *130*, 5854. (c) Hasegawa, S.; Horike, S.; Matsuda, R.; Furukawa, S.; Mochizuki, K.; Kinoshita, Y.; Kitagawa, S. *J. Am. Chem. Soc.* **2007**, *129*, 2607. (d) Horcajada, P.; Surblé, S.; Serre, C.; Hong, D.-Y.; Seo, Y.-K.; Chang, J.-S.; Grenèche, J.-M.; Margiolaki, I.; Férey, G. *Chem. Commun.* **2007**, 2820.

(4) (a) Uemura, T.; Hiramatsu, D.; Kubota, Y.; Takata, M.; Kitagawa, S. *Angew. Chem., Int. Ed.* **2007**, *46*, 4987. (b) Hermes, S.; Schröter, M.-K.; Schmid, R.; Khodeir, L.; Muhler, M.; Tissler, A.; Fischer, R. W.; Fischer, R. A. *Angew. Chem., Int. Ed.* **2005**, *44*, 6237.

 Published on Web 06/19/2009

is one of the most interesting phenomena in flexible PCPs.[1s,5,6] Such structural flexibility has been identified as a key principle for high selectivity, accommodation, and molecular sensing. Fundamental kinetic and thermodynamic studies on flexible PCPs have been recently performed to improve understanding and prediction of the behavior of flexible PCPs.[5c,6] Although a very strict control of the structural flexibility by a modification of coordination frameworks is the next challenging theme, there are few examples that have succeeded in such control.

To obtain such next-generation flexible PCPs, two types of interactions need to be considered. One is host−guest interaction, and the other is interaction acting between coordination frameworks. Here, we have focused on the polarity of the framework as a means of controlling these interactions. Introducing polar parts at the internal surface of porous frameworks is a very effective technique not only to enhance adsorption selectivity and enthalpy of adsorption for guests but also to change onset pressures. In other words, host−guest and host−host interactions can be controlled by the polarity. It has been found that in X and Y zeolites, cation-exchange affects the adsorption properties.[7] In the case of zeolites, the polarity of frameworks can be easily and systematically controlled using the cation-exchange method with retention of the original structure. Although highly selective uptake of targeted guests and the enhancement of enthalpy of adsorption derived from polar parts have been reported in some PCPs,[8] few strategies to introduce a polar part rationally into coordination frameworks have appeared to date.

One way to construct flexible coordination polymers is to use low-dimensional coordination frameworks. One- and two-dimensional coordination polymers seem to have more flexible frameworks than three-dimensional coordination polymers, because coordination bonds extend in restricted directions. Other weak interactions, such as hydrogen bonds, $\pi-\pi$, electrostatic, and van der Waals interactions, play an important role in stabilizing the assembled structures in one- and two-dimensional coordination polymers. However, little attention has so far been paid to the adsorption properties of one-dimensional coordination compounds, compared with high-dimensional coordination polymers, because of the lack of studies on such compounds.[1q,9,10]

One aspect of the sustainable development of our society is associated with the environmentally friendly and economically favorable separation, capture, and storage of small gas molecules, e.g., H_2, CO_2, CH_4, etc. CO_2 is the main component of greenhouse gases and would trigger severe global climate change if it accumulated to a high level in the long run. CO_2 is also a necessary intermediate product in most of the H_2 production processes. Hence, separation and storage of CO_2 from the flue exhaust of plants will be increasingly important in the future world environment.

From such viewpoints, we here studied the CO_2 gas adsorption properties of the one-dimensional coordination polymer $[Cu(PF_6)_2(bpetha)_2]_n$ (**1**; bpetha = 1,2-bis(4-pyridyl)ethane) with the controllable polar units, Cu−PF_6, as shown in Figure 1.[11] It has been reported that the combination of Cu^{II} ions showing the Jahn−Teller effect and the PF_6^- anion, known as a very weak Lewis base, affords weak and flexible Cu−PF_6 bonds.[11,12] The weak coordination of the PF_6^- anion to the cationic Cu^{II} ion and the presence of highly electronegative fluorine atoms enable the formation of the polar Cu−PF_6 unit that acts as a specific adsorption site for polar gases.[13] Moreover, the PF_6^- anions can be easily exchanged with other anions or neutral guests, because of the weak and flexible nature of the Cu−PF_6 bonds. Therefore, the Cu−PF_6 bond could become a useful building unit for the construction of next-generation flexible PCPs. In fact, **1** showed highly selective and unique CO_2 gas adsorption

(5) (a) Kitaura, R.; Seki, K.; Akiyama, G.; Kitagawa, S. *Angew. Chem., Int. Ed.* **2003**, *42*, 428. (b) Kondo, A.; Noguchi, H.; Ohnishi, S.; Kajiro, H.; Tohdoh, A.; Hattori, Y.; Xu, W.-C.; Tanaka, H.; Kanoh, H.; Kaneko, K. *Nano Lett*. **2006**, *6*, 2581. (c) Tanaka, D.; Nakagawa, K.; Higuchi, M.; Horike, S.; Kubota, Y.; Kobayashi, T. C.; Takata, M.; Kitagawa, S. *Angew. Chem., Int. Ed.* **2008**, *47*, 3914. (d) Bourrelly, S.; Llewellyn, P. L.; Serre, C.; Millange, F.; Loiseau, T.; Férey, G. *J. Am. Chem. Soc*. **2005**, *127*, 13519.

(6) Coudert, F.-X.; Jeffroy, M.; Fuchs, A. H.; Boutin, A.; Mellot-Draznieks, C. *J. Am. Chem. Soc*. **2008**, *130*, 14294.

(7) (a) Dunne, J. A.; Rao, M.; Sircar, S.; Gorte, R. J.; Myers, A. L. *Langmuir* **1996**, *12*, 5896. (b) Walton, K. S.; Abney, M. B.; LeVan, M. D. *Microporous Mesoporous Mater*. **2006**, *91*, 78. (c) Zhang, S. K.; Talu, O.; Hayhurst, D. T. *J. Phys. Chem*. **1991**, *95*, 1722.

(8) (a) Rowsell, J. L. C.; Spencer, E. C.; Eckert, J.; Howard, J. A. K.; Yaghi, O. M. *Science* **2005**, *309*, 1350. (b) Han, S. S.; Goddard, W. A. III. *J. Am. Chem. Soc*. **2007**, *129*, 8422. (c) Pan, L.; Adams, K. M.; Hemandez, H. E.; Wang, X.; Zheng, C.; Hattori, Y.; Kaneko, K. *J. Am. Chem. Soc*. **2003**, *125*, 3062.

(9) (a) Kachi-Terajima, C.; Akatsuka, T.; Kohbara, M.; Takamizawa, S. *Chem. Asian J*. **2007**, *2*, 40. (b) Takamizawa, S.; Hiroki, T.; Nakata, E.; Mochizuki, K.; Mori, W. *Chem. Lett*. **2002**, 1208. (c) Takamizawa, S.; Nakata, E.; Yokoyama, H. *Inorg. Chem. Commun*. **2003**, *6*, 763. (d) Nukada, R.; Mori, W.; Takamizawa, S.; Mikuriya, M.; Handa, M.; Naono, H. *Chem. Lett*. **1999**, 367. (e) Takamizawa, S.; Nakata, E.; Saito, T.; Kojima, K. *CrystEngComm* **2003**, *6*, 411. (f) Takamizawa, S.; Nakata, E.; Saito, T. *Inorg. Chem. Commun*. **2003**, *6*, 1415. (g) Takamizawa, S.; Nakata, E.; Saito, T. *Inorg. Chem. Commun*. **2004**, *7*, 1. (h) Takamizawa, S.; Nakata, E.; Saito, T. *Chem. Lett*. **2004**, 538. (i) Takamizawa, S.; Nakata, E. *CrystEngComm* **2005**, *7*, 476. (j) Takamizawa, S.; Nakata, E.; Saito, T.; Akatsuka, T.; Kojima, K. *CrystEngComm* **2004**, *6*, 197. (k) Takamizawa, S.; Saito, T.; Akatsuka, T.; Nakata, E. *Inorg. Chem*. **2005**, *44*, 1421. (l) Takamizawa, S.; Nakata, E.; Saito, T.; Akatsuka, T. *Inorg. Chem*. **2005**, *44*, 1362. (m) Takamizawa, S.; Kojima, K.; Akatsuka, T. *Inorg. Chem*. **2006**, *45*, 4580. (n) Takamizawa, S.; Nakata, E.; Saito, T. *Angew. Chem., Int. Ed*. **2004**, *43*, 1368. (o) Takamizawa, S.; Nakata, E.; Yokoyama, H.; Mochizuki, K.; Mori, W. *Angew. Chem., Int. Ed*. **2003**, *42*, 4331. (p) Takamizawa, S.; Kachi-Terajima, C.; Kohbara, M.; Akatsuka, T.; Jin, T. *Chem. Asian J*. **2007**, *2*, 837. (q) Ueda, T.; Kurokawa, K.; Eguchi, T.; Kachi-Terajima, C.; Takamizawa, S. *J. Phys. Chem. C* **2007**, *111*, 1524. (r) Goto, M.; Furukawa, M.; Miyamoto, J.; Kanoh, H.; Kaneko, K. *Langmuir* **2007**, *23*, 5264. (s) Kitagawa, S. *Nature* **2006**, *441*, 584.

(10) (a) Soldatov, D. V.; Moudrakovski, I. L.; Ratcliffe, C. I.; Dutrisac, R.; Ripmeester, J. A. *Chem. Mater*. **2003**, *15*, 4810. (b) Cingolani, A.; Galli, S.; Masciocchi, N.; Pandolfo, L.; Pettinari, C.; Sironi, A. *J. Am. Chem. Soc*. **2005**, *127*, 6144. (c) Uemura, K.; Saito, K.; Kitagawa, S.; Kita, H. *J. Am. Chem. Soc*. **2006**, *128*, 16122.

(11) Noro, S.; Horike, S.; Tanaka, D.; Kitagawa, S.; Akutagawa, T.; Nakamura, T. *Inorg. Chem*. **2006**, *45*, 9290.

(12) (a) Noro, S.; Kitaura, R.; Kondo, M.; Kitagawa, S.; Ishii, T.; Matsuzaka, H.; Yamashita, M. *J. Am. Chem. Soc*. **2002**, *124*, 2568. (b) Noro, S.; Yanai, N.; Kitagawa, S.; Akutagawa, T.; Nakamura, T. *Inorg. Chem*. **2008**, *47*, 7360.

(13) Some porous coordination polymers with organic ligands decorated with the fluorous atoms have been synthesized to enhance surface properties such as guest affinity and selectivity (a) Yang, C.; Wang, X.; Omary, M. A. *J. Am. Chem. Soc*. **2007**, *129*, 15454. (b) Kasai, K.; Aoyagi, M.; Fujita, M. *J. Am. Chem. Soc*. **2000**, *122*, 2140.

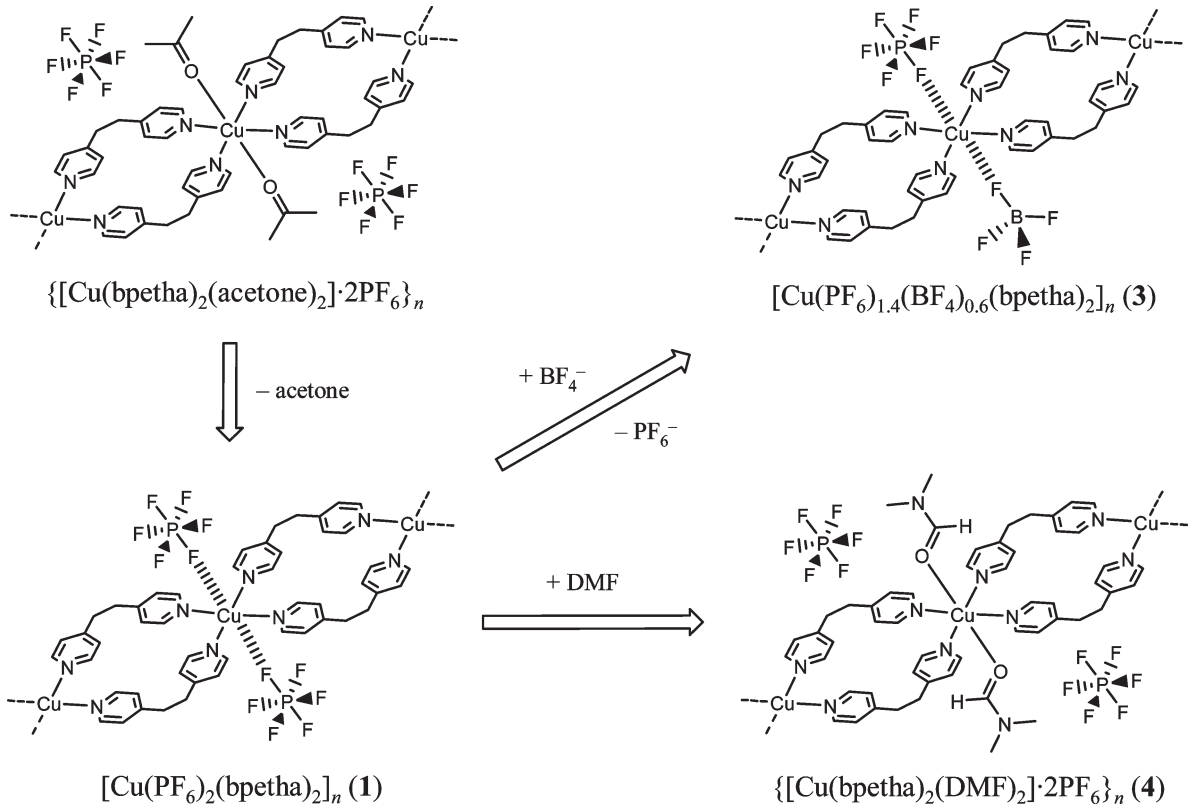

Figure 1. One-dimensional coordination polymers with weak and flexible Cu^{II} axial bonds.

properties derived from the polar Cu−PF_6 units and the flexibility of the one-dimensional system. Furthermore, the modification of the Cu−PF_6 units achieved tuning of the adsorption properties specifically for the targeted CO_2 gas.

Experimental Section

Materials. All reagents and chemicals were obtained from commercial sources. **1** was synthesized according to the literature.[11]

Synthesis of $[Cu(PF_6)_2(4\text{-mepy})_4]$ (2). An EtOH solution (30 mL) of 4-methylpyridine (4-mepy) (0.97 mL, 10.0 mmol) was added to a hot H_2O solution (50 mL) of $Cu(BF_4)_2\cdot 6H_2O$ (863 mg, 2.50 mmol) and KPF_6 (1.84 g, 10.0 mmol). The blue solution obtained was allowed to stand for two days, forming purple crystals. The crystals were filtered, washed with H_2O and EtOH, and dried in a vacuum at r.t. for 3 h. Yield 38%. Elemental anal. Calcd for $C_{24}H_{28}Cu_1F_{12}N_4P_2$: C, 39.71; H, 3.89; N, 7.72. Found: C, 39.13; H, 3.86; N, 7.62. IR (KBr pellet, cm^{-1}): 850 (PF_6^-).

Synthesis of $[Cu(PF_6)_{1.4}(BF_4)_{0.6}(bpetha)_2]_n$ (3). An acetone solution (20 mL) of bpetha (368 mg, 2.00 mmol) was added to a hot H_2O solution (20 mL) of $Cu(BF_4)_2\cdot 6H_2O$ (345 mg, 1.00 mmol) and KPF_6 (276 mg, 1.50 mmol). The purple microcrystals obtained were filtered, washed with H_2O and acetone, and dried in a vacuum at 393 K for 3 h. Yield 83%. **3** easily adsorbed H_2O guests from the atmosphere to form the hydrated compound $\mathbf{3}\cdot x H_2O$. Elemental anal. Calcd for $C_{24}H_{25.8}B_{0.6}Cu_1F_{10.8}N_4O_{0.9}P_{1.4}$ ($\mathbf{3}\cdot 0.9H_2O$): C, 40.99; H, 3.70; N, 7.97. Found: C, 41.21; H, 3.66; N, 7.95. IR (KBr pellet, cm^{-1}): ~1100 (broad, BF_4^-) and 847 (PF_6^-).

Synthesis of $\{[Cu(bpetha)_2(DMF)_2]\cdot 2PF_6\}_n$ (4). Single crystals of **4** have already been synthesized and crystallographically characterized.[11] In this article, we employed a postsynthetic modification to obtain microcrystals of **4**.[1t,14] **1** (50 mg, 6.93×10^{-2} mmol) was exposed to DMF vapor for one day. The sky-blue powder obtained was dried in vacuum at r.t. for 3 h. Elemental analysis calcd for $C_{30}H_{38}Cu_1F_{12}N_6O_2P_2$ (**4**): C, 41.51; H, 4.41; N, 9.68. Found: C, 41.40; H, 4.31; N, 9.65. IR (KBr pellet, cm^{-1}): 1660 (C=O) and 841 (PF_6^-).

X-ray Structural Analysis. X-ray diffraction measurement of **2** was performed using a Rigaku RAXIS-RAPID imaging plate diffractometer using graphite-monochromated Mo Kα radiation ($\lambda = 0.71073$ Å). The data were corrected for Lorentz and polarization effects. The structure was solved using direct methods (SIR2004)[15] and expanded using Fourier techniques.[16] All nonhydrogen atoms were refined anisotropically. All of the hydrogen atoms were refined using the riding model. The refinements were carried out using full-matrix least-squares techniques on F^2. All calculations were performed using the CrystalStructure crystallographic software package.[17] The crystal data are summarized in Table 1. The crystallographic data in CIF format are available from the Cambridge Crystallographic Data Centre, CCDC reference number 703702.

(14) (a) Seo, J. S.; Whang, D.; Lee, H.; Jun, S. I.; Oh, J.; Jeon, Y. J.; Kim, K. *Nature* **2000**, *404*, 982. (b) Wang, Z.; Cohen, S. M. *J. Am. Chem. Soc.* **2007**, *129*, 12368. (c) Ingleson, M. J.; Barrio, J. P.; Guilbaud, J.-B.; Khimyak, Y. Z.; Rosseinsky, M. J. *Chem. Commun.* **2008**, 2680. (d) Hwang, Y. K.; Hong, D.-Y.; Chang, J.-S.; Jhung, S. H.; Seo, Y.-K.; Kim, J.; Vimont, A.; Daturi, M.; Serre, C.; Férey, G. *Angew. Chem., Int. Ed.* **2008**, *47*, 4144.

(15) Burla, M. C.; Caliandro, R.; Camalli, M.; Carrozzini, B.; Cascarano, G. L.; De Caro, L.; Giacovazzo, C.; Polidori, G.; Spagna, R. SIR2004; Istituto di Cristallografia: Bari, Italy, **2005**.

(16) Beurskens, P. T.; Admiraal, G.; Beurskens, G.; Bosman, W. P.; de Gelder, R.; Israel, R.; Smits, J. M. M. DIRDIF-99 Program System, Technical Report of the Crystallography Laboratory; University of Nijmegen: Nijmegen, The Netherlands, 1999.

(17) CrystalStructure 3.8: Crystal Structure Analysis Package; Rigaku and Rigaku Americas: The Woodlands, TX, 2000−2007.

Table 1. Crystallographic Data for 2

formula	$C_{48}H_{56}Cu_2F_{24}N_8P_4$
fw	1451.97
lattice	triclinic
a (Å)	10.9807(6)
b (Å)	16.9871(7)
c (Å)	17.3239(7)
α (deg)	81.013(2)
β (deg)	82.301(2)
γ (deg)	75.058(2)
V (Å^3)	3068.9(2)
space group	$P\bar{1}$
Z	2
ρ(calcd) (g cm^{-3})	1.571
F(000)	1468.00
μ (Mo Kα) (cm^{-1})	9.110
radiation (λ, Å)	0.71073
T (K)	173
R^a	0.0353
$R_w{}^b$	0.0591
GOF	1.064
no. of observations	7620
no. of variables	831

$^a R = \Sigma||F_o| - |F_c||/\Sigma|F_o|$. $^b R_w = [\Sigma w(|F_o| - |F_c|)^2/\Sigma w F_o^2]^{1/2}$.

Measurements. Elemental analysis (C, H, N) was performed on a PerkinElmer Model 240C elemental analyzer. IR spectra (400−4000 cm^{-1}) were recorded on a PerkinElmer Spectrum 2000 spectrometer with samples prepared as KBr pellets. Temperature-dependent microscopic IR spectra (650−4000 cm^{-1}) under gas flow were measured on Thermo Nicolet 6700 and Thermo Nicolet Continuum spectrometers with a Linkam FTIR600 heating and freezing stage. The samples were directly placed on the BaF_2 plate. X-ray diffraction (XRD) data at r.t. and in the atmosphere were collected on a Rigaku RINT-Ultima III using Cu Kα radiation. In situ synchrotron radiation experiments were performed at SPring-8 with the approval of JASRI. Thermogravimetry−differential thermal analysis (TG−DTA) was performed on a Rigaku Thermo Plus 2/TG8120 over the temperature range 298−573 K at a heating rate of 10 K/min in an N_2 atmosphere. Solid-state static and magic angle spinning (MAS) ^{19}F-NMR experiments were carried out on a BRUKER DSX300 spectrometer operating at a resonance frequency of 282.2 MHz. The spectra were obtained by solid-echo $\pi/2(\phi_1)-\tau-\pi/2(\phi_2)$ and spin−echo pulse sequence $\pi/2(\phi_1)-\tau-\pi(\phi_2)$ synchronized with the MAS speed at 25 kHz for static and MAS NMR, respectively. ^{19}F shifts were referenced to $CFCl_3$ (0 ppm), and 4-fluorobenzotrifluoride was used as a second external reference sample. Temperature-dependent ESR spectra were measured using a JEOL JES FA-100 spectrometer equipped with a temperature control system (Oxford ESR900 cryostat). The microcrystalline sample was set in a quartz sample tube. The g-values of the ESR signals were corrected at the third and fourth reference signals of MnO. UV−vis reflection spectra were recorded using a Hitachi U-3500 spectrophotometer with a resolution of 0.5 nm. The adsorption isotherms of CO_2 and C_2H_2 gas at 195 K were measured with an automatic volumetric adsorption apparatus (Autosorb-1; Quantachrome Instruments). The adsorption isotherms of N_2 and Ar at 77 K, and CO at 77 and 195 K, were performed with an automatic volumetric adsorption apparatus (BELSORP MAX; BEL Japan, Inc.). The adsorption isotherms of H_2 at 77 and 195 K were recorded using BELSORP-mini volumetric adsorption apparatus (BEL Japan, Inc.). The temperature-dependent adsorption isotherms of CO_2 gas were measured with BELSORP-18 volumetric adsorption equipment attached to a closed-cycle helium cryostat (BEL Japan, Inc.). The adsorption isotherms of CO_2 gas at high pressure and 298 K were measured on an FMS-BG (BEL Japan, Inc.) automatic gravimetric adsorption measurement system with Rebotherm magnet coupling balance incorporated in a SUS steel pressure chamber. Prior to the adsorption measurements, the samples were treated under reduced pressure ($< 10^{-2}$ Pa) at 353 K for 12 h.

Calculations. The DFT calculations were performed with the B3LYP/LanL2DZ basis set using the package Gaussian 03, revision D.01.[18] A natural population analysis (NPA) was used to obtain the charge distribution.[19] The B3LYP/LanL2DZ basis set has been used to compare the properties of coordination compounds.[20] The atomic coordinates of **2** and α-[Ni(NCS)$_2$(4-mepy)$_4$] based on the X-ray crystal structural analysis were used for the calculations.[21]

Results and Discussion

The desolvated compound **1** was obtained by removal of guest acetone molecules from $\{[Cu(bpetha)_2(acetone)_2]\cdot 2PF_6\}_n$ with the one-dimensional doubly linked chain structure shown in Figure 1.[11] The N_2 adsorption and desorption isotherms of **1** at 77 K show a typical type II curve, and the calculated BET specific surface area is 15 m^2 g^{-1}. This low specific surface area leads to the conclusion that N_2 molecules (kinetic diameter: 3.64 Å) could not diffuse into the framework of **1** at all. On the other hand, CO_2 adsorption and desorption isotherms of **1** at 195 K (Figure 2) show a profile unlike the usual adsorption patterns. **1** shows three-step adsorption with onset relative pressure of $\sim 10^{-2}$ (point A), 0.1 (point B), and 0.5 (point C). In the region from zero to point A, no CO_2 gas is adsorbed, supporting the absence of pores. In the region from point A to point B, the isotherm exhibits a gradual increase in the adsorption amount. The Langmuir surface area calculated from this region is 192 m^2 g^{-1}. These results indicate that a structural transformation occurs at point A and small pores are formed in **1** after the transformation. At the second and third steps, **1** further adsorbs CO_2 gas, forming intermediate compounds $\mathbf{1}\cdot 2CO_2$ and $\mathbf{1}\cdot 4CO_2$, respectively. This is similar to gate-opening-type adsorption behavior,[1s,5,6] which is related to the structural transformation of the host framework. By applying the Langmuir model, we found the apparent surface area to be 882 m^2 g^{-1}, a value that is comparable to the highest value for zeolites, zeolite Y (904 m^2 g^{-1}),[22] and larger than that of the one-dimensional PCP, $[Rh_2(benzoate)_2(pyrazine)]_n$ (353 m^2 g^{-1}).[9b] This high specific surface area clearly shows that nonporo us framework **1** is transformed into a porous framework.

(18) Frisch, M. J.et al. Gaussian 03, revision D.01; Gaussian, Inc.; Wallingford, CT, 2004.
(19) (a) Reed, A. E.; Weinhold, F. *J. Chem. Phys.* **1983**, *78*, 4066. (b) Reed, A. E.; Weinstock, R. B.; Weinhold, F. *J. Chem. Phys.* **1985**, *83*, 735.
(20) (a) Muckerman, J. T.; Polyansky, D. E.; Wada, T.; Tanaka, K.; Fujita, E. *Inorg. Chem.* **2008**, *47*, 1787. (b) Shieh, M.; Hsu, M.-H.; Sheu, W.-S.; Jang, L.-F.; Lin, S.-F.; Chu, Y.-Y.; Miu, C.-Y.; Lai, Y.-W.; Liu, H.-L.; Her, J. L. *Chem.—Eur. J.* **2007**, *13*, 6605.
(21) (a) Lipkowski, J. In Inclusion Compounds; Atwood, J. L., Davies, J. E. D., MacNicol, D. D., Eds.; Academic Press: New York, 1984; Vol. *1*, pp 59-103.(b) Soldatov, D. V.; Enright, G. D.; Ripmeester, J. A. *Cryst. Growth Des.* **2004**, *4*, 1185.
(22) Chester, A. W.; Clement, P.; Han, S. U.S. Patent Appl. 2000/6136291A, **2006**.

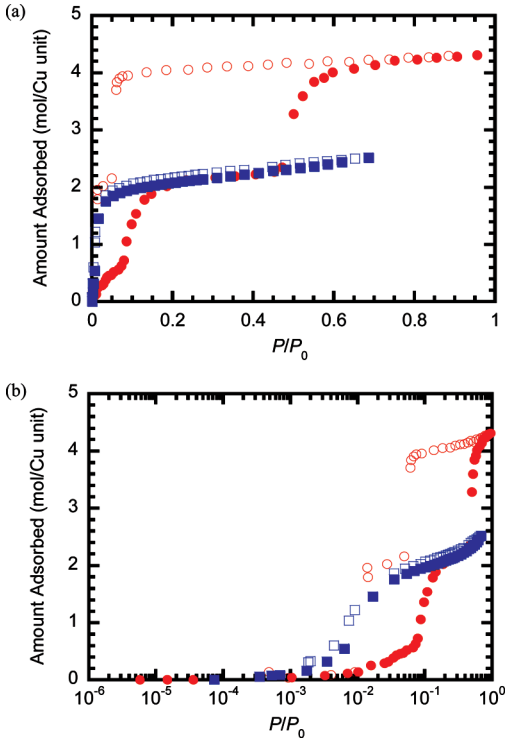

Figure 2. (a) Adsorption (filled symbols) and desorption (open symbols) isotherms for CO_2 (red) and C_2H_2 (blue) on **1** at 195 K. (b) Adsorption and desorption isotherms for CO_2 and C_2H_2 at 195 K plotted against a logarithmic relative pressure.

The desorption isotherm does not trace the adsorption isotherm any more, instead showing an abrupt drop at relative pressure 0.06 (point C′) and 0.01 (point B′). This sharp adsorption jump−desorption drop with a large hysteresis also indicates the occurrence of a framework transformation in the crystalline state. The adsorption/desorption process is reversible over many cycles. It is interesting that an integral number of CO_2 molecules is adsorbed at the second and third adsorption steps; that is, a commensurate adsorption occurs, supporting the presence of specific adsorption sites for guests. Because the Cu−PF_6 parts have the strongest polarity in the framework, it is expected that they act as specific adsorption sites for CO_2.

To obtain further information on the adsorption site for the CO_2 molecules, we measured the IR spectra of **1** at 293 and 200 K under CO_2 and N_2 flow (Figure 3). The spectra at 293 K under CO_2 flow are the same as those under N_2 flow, indicating that no adsorption occurs at this temperature. A new weak band at 2274 cm^{-1} was detected at 200 K under CO_2 flow. This is assigned to the $^{13}CO_2$ asymmetric stretching mode (ν_3), the intensity of which is about 100 times lower than that corresponding to the $^{12}CO_2$ ν_3.[23] The ν_3 band frequency is clearly lower than those observed in the pure gas and solid phases (2284.5 and 2282 cm^{-1}, respectively),[24] which is also

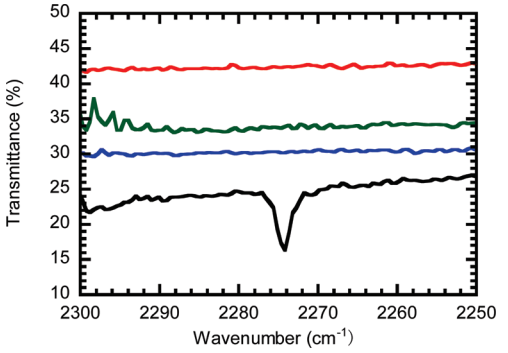

Figure 3. IR spectra of **1** under N_2 flow at 290 K (red), under N_2 flow at 200 K (blue), under CO_2 flow at 293 K (green), and under CO_2 flow at 200 K (black).

expected in the case of electron donor−acceptor complexes involving CO_2 as an electron acceptor.[25] The IR spectra of $[CuCl_2(bpetha)]_n$ (**5**), which shows no CO_2 adsorption property with a structural transformation (see Figure S18), were measured under similar conditions to confirm that the observed band is not derived from the adsorption of CO_2 to external surfaces of the crystals. The IR spectrum of **5** at 200 K under CO_2 flow has no ν_3 band (see Figure S19 in the Supporting Information), indicating that CO_2 adsorbed to the external surface has no relationship to the observed ν_3 band. Hence, these results support the belief that the adsorbed CO_2 interacts with electron-donor sites of the framework as an electron acceptor via its carbon atom.

To investigate the structure and polarity of the Cu−PF_6 part, $[Cu(PF_6)_2(4\text{-mepy})_4]$ (**2**) was synthesized as a compound with a basic $[Cu(PF_6)_2(pyridine)_4]$ structure and characterized using single-crystal X-ray diffraction analysis, UV−vis reflection spectra, and DFT calculations. In the crystal, there are two crystallographically independent Cu^{II} complexes (I and II), both of which have similar coordination environments. The structure of the Cu^{II} complex I in **2** is shown in panels a and b in Figure 4. The Cu^{II} ion has an elongated octahedral environment with four 4-mepy nitrogen atoms in the equatorial plane, and two fluorine atoms of the PF_6^- anions at the axial sites. Each Cu^{II} complex adopts a propeller-type conformation, because of steric hindrance between the hydrogen atoms of the 4-mepy pyridine rings. Such a conformation is similar to that in **1** with guests.[11] The Cu−F bond distances (2.586(2) and 2.528(2) Å for complex I, and 2.478(2) and 2.629(2) Å for complex II) are considerably longer than the Cu−N bond distances (2.002−2.024 Å), indicative of a Jahn−Teller effect. The UV−vis reflection spectrum of **2** (Figure S1) has a broad peak with an absorption maximum at 19.5×10^3 cm^{-1}, a value that is similar to that of **1** (19.1×10^3 cm^{-1}, see Figure S1 in the Supporting Information). These results indicate that the coordination environments around the Cu^{II} centers in **1** and **2** are similar to each other. From the

(23) Under our experimental conditions, we could not obtain information on the $^{12}CO_2$ ν_3 bands, which are commonly used as a reference to check whether CO_2 acts as an electron donor or electron acceptor.

(24) (a) Herzberg, G. Molecular Spectra and Molecular Structure; van Nostrand Reinhold: New York, 1950.(b) Gálvez, Ó.; Maté, B.; Herrero, V. J.; Escribano, R. *Icarus* **2008**, *197*, 599.

(25) (a) Weber, J. M.; Schneider, H. *J. Chem. Phys.* **2004**, *120*, 10056. (b) Vimont, A.; Travert, A.; Bazin, P.; Lavalley, J.-C.; Daturi, M.; Serre, C.; Férey, G.; Bourrelly, S.; Llewellyn, P. L. *Chem. Commun.* **2007**, 3291.

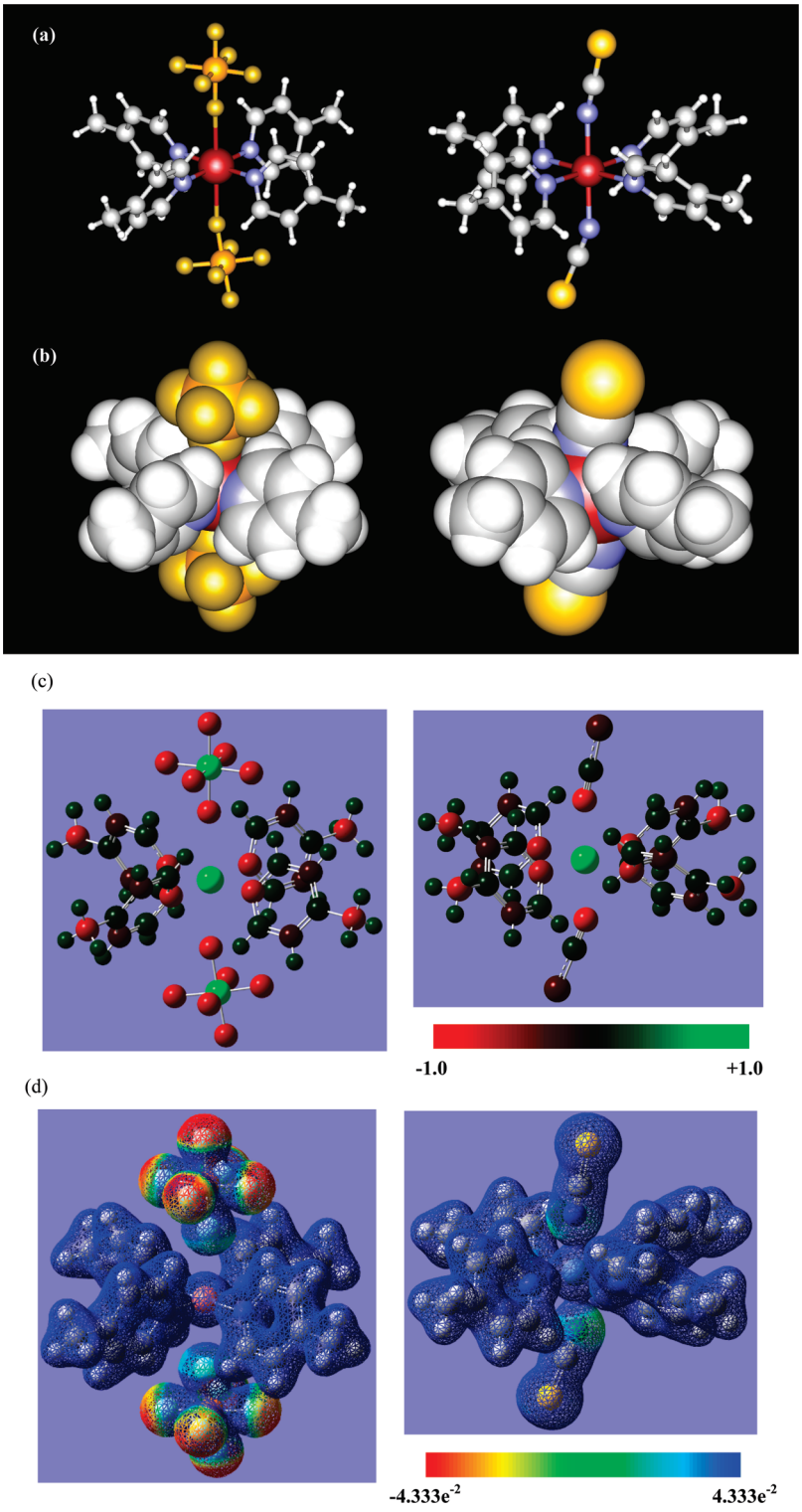

Figure 4. (a) Structures, (b) CPK representations, (c) visualized charge distributions, and (d) electrostatic surface potentials mapped onto a surface of total electron density of **2** (left) and α-[Ni(NCS)$_2$(4-mepy)$_4$] (right).

structural data of **2**, we calculated the natural charges using NPA. The natural charges of the Werner complex α-[Ni(NCS)$_2$(4-mepy)$_4$] (panels a and b in Figure 4),[21] which has no Jahn−Teller bonds (Ni−N(NCS) bond distances = 2.068(2) and 2.071(2) Å), were also evaluated to compare the polarity. Visualized charge distributions are shown in Figure 4c and selected natural charges are listed in Table 2. In the case of **2**, the total charge of the PF_6^- anions is in the range from −0.95875 to −0.96064, values that are very similar to the ideal value, −1. On the other hand, the corresponding values of the NCS^- anions in α-[Ni(NCS)$_2$(4-mepy)$_4$] (−0.75313 and −0.75608) are considerably smaller than −1. Furthermore, the coordination-free F atoms of the PF_6^- anions, which are seen to be on the surface of the Cu^{II} complexes as shown in Figure 4b, have larger negative charges than the

Table 2. Selected Natural Charges from the NPA Analysis[a]

2					
complex I		complex II		α-[Ni(NCS)$_2$(4-mepy)$_4$]	
Cu(1)	1.34135	Cu(2)	1.34235	Ni(1)	1.37800
P(1)	2.83653	P(3)	2.83228	N(1)	−0.73206
P(2)	2.83920	P(4)	2.83434	C(1)	0.11395
F(1)	−0.66284	F(13)	−0.66435	S(1)	−0.25708
F(2)	−0.62077	F(14)	−0.61435	N(2)	−0.72208
F(3)	−0.62943	F(15)	−0.62755	C(2)	0.11681
F(4)	−0.62766	F(16)	−0.62983	S(2)	−0.26737
F(5)	−0.62816	F(17)	−0.62730	N(3)	−0.57096
F(6)	−0.62772	F(18)	−0.62765	N(4)	−0.56122
F(7)	−0.66510	F(19)	−0.66166	N(5)	−0.56766
F(8)	−0.61486	F(20)	−0.61858	N(6)	−0.56190
F(9)	−0.62928	F(21)	−0.63143		
F(10)	−0.63102	F(22)	−0.62601		
F(11)	−0.63221	F(23)	−0.63053		
F(12)	−0.62589	F(24)	−0.62677		
N(1)	−0.60713	N(5)	−0.60717		
N(2)	−0.60191	N(6)	−0.60066		
N(3)	−0.60650	N(7)	−0.60609		
N(4)	−0.60548	N(8)	−0.60419		

[a] The numbering schemes of the unique atoms are shown in Figure S2 of the Supporting Information.

coordination-free S atoms in α-[Ni(NCS)$_2$(4-mepy)$_4$]. The electrostatic surface potentials mapped onto a surface of total electron density (Figure 4d) also support the more polar framework of **1**. The results of the calculations clearly indicate that **1** has a polar structure derived from the Cu−PF_6 parts. The charge distribution of the framework obtained from the calculations and the ν_3 band of the adsorbed CO_2 implies that the F atoms of the PF_6^- anions act as electron donors and interact with electron-acceptor CO_2 molecules. This is unprecedented because the PF_6^- anion is a very weak Lewis base.[12b] The formation of electron donor−acceptor interactions should be attributed to the strong confinement effect of the nanospace.

We also measured the adsorption isotherms of C_2H_2 gas at 195 K (Figure 2). CO_2 and C_2H_2 molecules are similar to one another in equilibrium sorption parameters, related physicochemical properties, and molecular size and shape (see Table S1 in the Supporting Information). The different parameters in these molecules are the magnitudes of the quadrupole moment and the polarizability. CO_2 possesses a quadrupole moment of -14.9×10^{-40} C m^2 and a polarizability of 2.911×10^{-24} cm^3, values that are smaller than those of C_2H_2 ($+25.1 \times 10^{-40}$ C m^2 and 3.33×10^{-24} cm^3). C_2H_2 also has acidic hydrogen atoms at both ends ($pK_a = 25$) that act as hydrogen-bonding sites.[26] If electrostatic and electron donor−acceptor interactions contribute to the adsorption of CO_2 and C_2H_2 in **1**, the adsorption and desorption isotherms of CO_2 and C_2H_2 should show different shapes from each other. The observed isotherms of CO_2 and C_2H_2 (Figure 2) are consistent with our expectation. **1** shows two-step adsorption with onset relative pressures of $\sim 1 \times 10^{-3}$ (point A) and $\sim 1 \times 10^{-2}$ (point B). In the region from zero to point A, no C_2H_2 gas is adsorbed, supporting the absence of pores. In the region from point A to point B, the isotherm exhibits a gradual increase in the adsorption amount. At the second step, **1** strongly adsorbs C_2H_2 gas, forming **1**·2C_2H_2. By applying the Langmuir model, we found the apparent surface area to be 425 m^2 g^{-1}, a value that is half the value for CO_2. No further structural transformation is induced by an increase in pressure, suggesting strong interactions between the host framework and guest C_2H_2 molecules. The structural stabilization of **1**·2C_2H_2 by such interactions prevents the additional insertion of C_2H_2 with structural transformation. The first and second onset pressures for C_2H_2 are lower than those for CO_2, which also indicates that the C_2H_2 molecules interact strongly with the host frameworks. The one-dimensional frameworks have an anionic surface originating from the weakly coordinated PF_6^- anions as mentioned above. Therefore, it is reasonable that C_2H_2 molecules, with their larger quadrupole moment, polarizability, and acidic protons, interact strongly with the host framework.

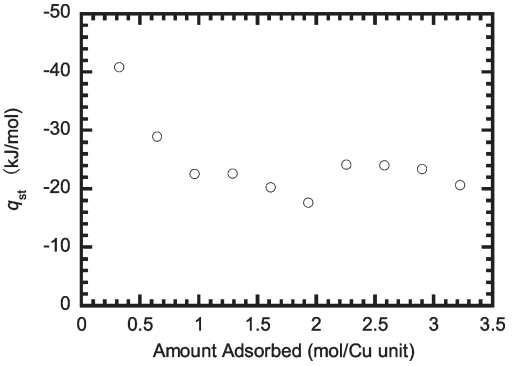

Figure 5. Calculated isosteric heat of adsorption of CO_2 on **1** plotted against the amount adsorbed.

The isosteric heat of adsorption of CO_2 was calculated according to the following equation using CO_2 adsorption isotherms measured at 185, 190, and 195 K (Figure 5)

$$q_{st} = -R\left(\frac{\partial \ln P}{\partial (1/T)}\right)_N$$

where q_{st}, R, P, and N represent the isosteric heat of adsorption, gas constant, pressure, and the amount of adsorption of CO_2, respectively. The value of q_{st} extrapolated to zero loading is ca. −50 kJ mol^{-1}, which is much greater than the values for physisorption on mesoporous silicas ($\sim$ −20 kJ mol^{-1})[27] and comparable with the values of NaX and Na-ZSM-5 with Na^+ ions providing strong ion charge density (−49.1 and −50.0 kJ mol^{-1}, respectively),[28] supporting the effect of the polar Cu−PF_6 sites and the micropore filling. On the other hand, the values for amounts of adsorption greater than 20 cm^3 g^{-1} are small and almost constant (approximately −20 kJ mol^{-1}). This relatively weak interaction with **1** suggests that the structural transformations occurring at the second

(26) Matsuda, R.; Kitaura, R.; Kitagawa, S.; Kubota, Y.; Relosludov, R. V.; Kobayashi, T. C.; Sakamoto, H.; Chiba, T.; Takata, M.; Kawazoe, Y.; Mita, Y. *Nature* **2005**, *436*, 238.

(27) Katoh, M.; Sakamoto, K.; Kamiyamane, M.; Tomida, T. *Phys. Chem. Chem. Phys.* **2000**, *2*, 4471.

(28) Dunne, J. A.; Rao, M.; Sircar, S.; Gorte, R. J.; Myers, A. L. *Langmuir* **1996**, *12*, 5896.

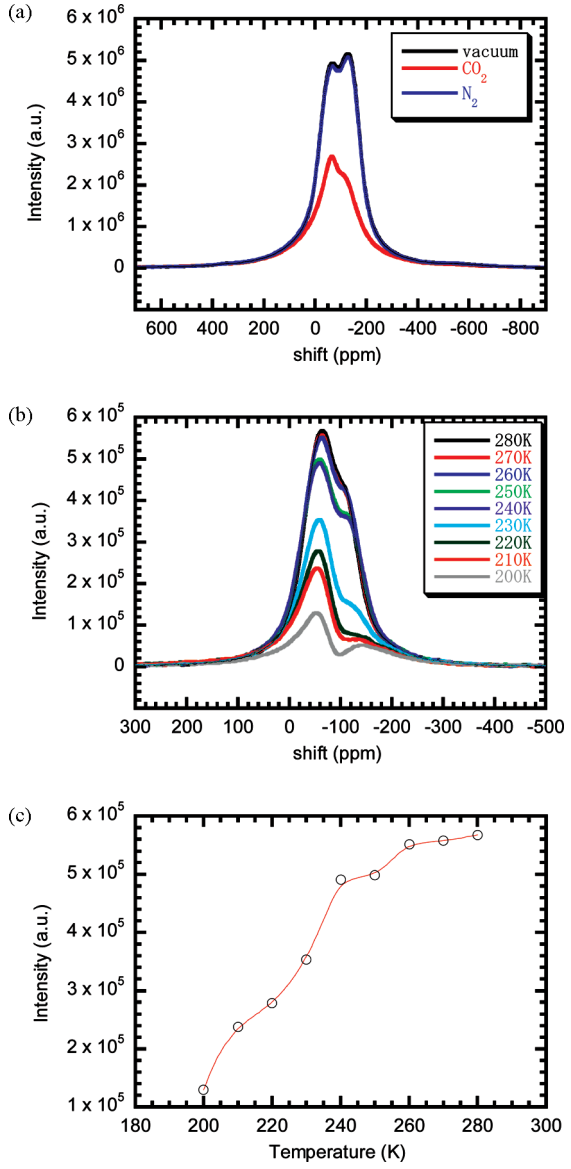

Figure 6. Solid-state static ^{19}F-NMR spectra in **1**. (a) Spectra at 200 K under vacuum (black) and 1 atm of CO_2 (red) and N_2 (blue). The spectra under vacuum overlap those under 1 atm of N_2. (b) Temperature dependence of the spectra under 1 atm of CO_2. (c) Temperature dependence of the spectral intensities under 1 atm of CO_2.

and third steps do not need strong host−guest interactions. In other words, the assembly of one-dimensional frameworks is very flexible, which is a unique character of low-dimensional coordination compounds.

To check the states of both the one-dimensional framework and its assembled form after CO_2 adsorption, we measured the temperature dependence of solid-state static ^{19}F-NMR spectra in a variety of atmospheres and vacuum. At room temperature and in air, the spectra have an anisotropic form because the PF_6^- anions approach the paramagnetic Cu^{II} centers. As the temperature decreases, the degree of the spectral anisotropy increases because of the presence of the adjacent Cu^{II} spins (Figure S3). In a N_2 atmosphere or in vacuum, the ^{19}F-NMR spectra at 200 K are almost identical to each other, indicative of no adsorption on the internal space of **1**. On the other hand, the ^{19}F-NMR spectra in a CO_2 atmosphere are clearly

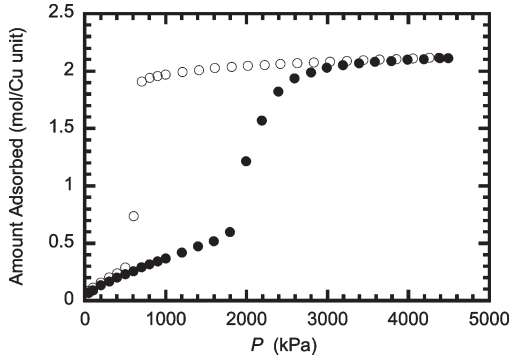

Figure 7. Adsorption (filled symbols) and desorption (open symbols) isotherms for CO_2 on **1** at 298 K.

different from those in a N_2 atmosphere and vacuum: the echo signal intensity in a CO_2 atmosphere is weaker than those in a N_2 atmosphere and vacuum (Figure 6a), when the same solid-echo pulse sequence $\pi/2(\phi_1)-\tau-\pi/2(\phi_2)$ with $\pi/2 = 2.8$ μs and $\tau = 8$ μs was used for all of the samples under the different atmospheres. By measuring under a variety of conditions, it is clarified that the relaxation time of the ^{19}F nuclear spin becomes quite short after the adsorption of CO_2. Furthermore, the temperature dependence of the ^{19}F-NMR spectra in a CO_2 atmosphere (Figure 6b), which was measured with $\pi/2 = 2.5$ μs and $\tau = 1$ μs, shows a discontinuous decrease in spectral intensity with decrease in temperature, and a three-stage change is clearly observed in the plot of spectral intensity vs temperature (Figure 6c). As mentioned above, the adsorption isotherm of CO_2 shows a three-step jump. Hence, the adsorption of CO_2 in **1** causes a change in the echo signal intensity of ^{19}F-NMR. If the distance between the PF_6^- anion and the paramagnetic Cu^{II} ion decreases by adsorption of CO_2, the relaxation time T_2 should decrease and the line width should increase. However, the observed line width is almost the same in N_2 and CO_2 atmospheres. Therefore, it is expected that T_2 is unchanged; that is, the adsorption of CO_2 in **1** scarcely has an effect on the Cu−PF_6 distance. We next measured the temperature dependence of the ESR spectra in N_2 and CO_2 atmospheres to check the change of the spin state of the Cu^{II} ions. In a N_2 atmosphere, the $g_\perp$ value is almost constant (2.064) and the integrated intensity gradually decreases with increase in temperature (see Figure S4 in the Supporting Information), indicating a constancy of the coordination environment around the Cu^{II} center, which is in good agreement with the results of the adsorption/desorption isotherms of N_2 and ^{19}F-NMR spectra under a N_2 atmosphere. On the other hand, in a CO_2 atmosphere, the $g_\perp$ value changes slightly from 2.062 to 2.064 and the integrated intensity increases with increase in temperature from 220 to 240 K (see Figure S5 in the Supporting Information). Therefore, the results of the ESR spectra strongly suggest that the spin state of Cu^{II} ions undergoes a change upon CO_2 adsorption and this change in the Cu^{II} spin state makes the spin−lattice relaxation time T_1 of the ^{19}F nuclear spin too short to detect all of the echo signal intensity. The reason for the change may be an expansion of the interchain Cu···Cu

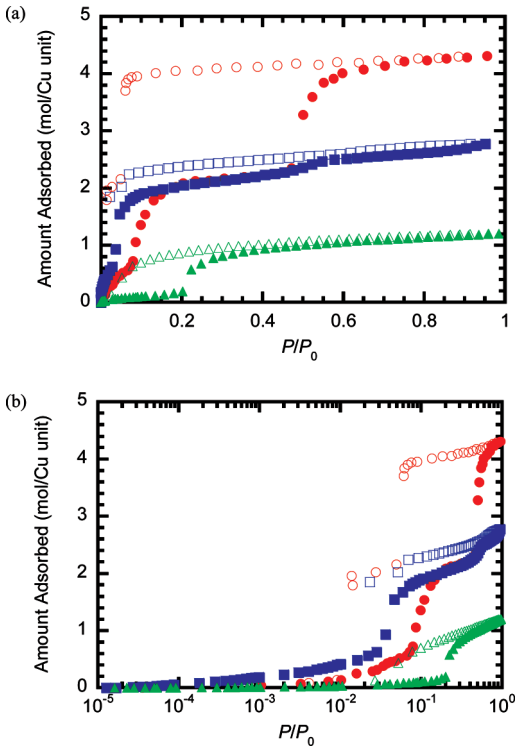

Figure 8. (a) Adsorption (filled symbols) and desorption (open symbols) isotherms for CO_2 on **1** (red), **3** (blue), and **4** (green) at 195 K. (b) Adsorption and desorption isotherms for CO_2 at 195 K plotted against a logarithmic relative pressure.

distance by CO_2 adsorption; that is, structural transformations. When the Cu···Cu distance lengthens by CO_2 adsorption, the antiferromagnetic interaction between Cu^{II} ions weakens and the paramagnetic character increases. As a consequence, the up−down motion of spins becomes active, which enhances the spin−lattice relaxation of the F nuclei. To confirm the structural transformations upon CO_2 adsorption, we determined the temperature dependence of the XRD patterns under a CO_2 atmosphere (see Figure S6 in the Supporting Information). The XRD results are consistent with the results of NMR and ESR spectra. The XRD patterns of **1** at 300 K and 31.9 kPa of CO_2 are similar to that at 410 K in a vacuum, indicating that no CO_2 adsorption occurs at this temperature and pressure. On the other hand, after cooling from 300 to 200 K under a CO_2 atmosphere, the XRD pattern is different from the former pattern. By maintaining at 200 K for 30 min under a CO_2 atmosphere, the XRD pattern shows further change. Because the pressure (31.9 kPa) is higher than the first and second onset pressures (points A and B) and lower than the third onset pressure (point C) as mentioned above, the observed two-step change corresponds well with the experimental adsorption.

CO_2 adsorption isotherms were also obtained at 298 K (Figure 7). The observed isotherms have a two-step adsorption jump and are similar to those at 195 K, indicating that structural transformations occur at room temperature. Although the onset pressure (~1.8 MPa) is still high for application as a CO_2 adsorbent, this pressure can be controlled by modifying the Cu−PF_6 part (see below).

Next, we measured the adsorption isotherms of N_2, O_2, CO, and H_2, in **1** at 195 K to evaluate the separation ability. The adsorption and desorption isotherms of N_2, O_2, CO, and H_2, at 195 K (see Figure S7 in the Supporting Information) show a type II curve, indicative of no structural transformation to a porous form. The volume ratios of adsorbed CO_2/N_2, CO_2/O_2, CO_2/CO, and CO_2/H_2, at 195 K and ~20 kPa are 8500, 2600, 100, and 1800, respectively. These results indicate that **1** is a good candidate for novel CO_2 separation materials. We also measured the adsorption isotherms of Ar, CO, and H_2, at 77 K (see Figures S8 and S9 in the Supporting Information). However, no adsorption was observed for any gases. As shown in Table S1, which lists the molecular size and physical parameters of the gases, the molecular size and the strength of electrostatic interactions are not crucial factors in determining the selectivity, because the smaller H_2 and more polar CO are not adsorbed. CO_2 and C_2H_2 can act as electron acceptors and interact with electron-donor sites via electron donor−acceptor interactions, which may contribute to adsorption selectivity.

If the Cu−PF_6 part strongly influences the adsorption properties for CO_2 and C_2H_2, modification of the Cu−PF_6 part may be a useful method to change the adsorption properties drastically. From this viewpoint, an exchange in the axial ligands in **1** was performed, forming the two derivatives, $[Cu(PF_6)_{1.4}(BF_4)_{0.6}(bpetha)_2]_n$ (**3**) and $\{[Cu(bpetha)_2(DMF)_2]\cdot 2PF_6\}_n$ (**4**) (Figure 1). **3** has both PF_6^- and BF_4^- anions in the framework. XRD patterns of **3** and **3** after exposure to acetone vapor are similar to the corresponding XRD patterns of **1** (see Figure S13 in the Supporting Information), indicative of the formation of a one-dimensional doubly linked chain structure. Because the Lewis basicity of a BF_4^- anion is greater than that of a PF_6^- anion,[12b] the Cu−BF_4 bond distance is shorter than the Cu−PF_6 bond distance, which was checked by the ^{19}F-NMR spectra and the TG−DTA of **3** with acetone guests (see Figures S10 and S11 in the Supporting Information). The adsorption isotherms of CO_2 on **3** (Figure 8) show three-step adsorption with onset relative pressures of $\sim 1 \times 10^{-3}$ (point A), $\sim 2 \times 10^{-2}$ (point B), and 0.5 (point C). In the region from point A to point B, the isotherm exhibits a gradual increase in the adsorption amount. At the second step, **3** further adsorbs CO_2 gas, forming **3**·2CO_2. At the third step, **3**·2CO_2 adsorbs a small number of CO_2 molecules. The first and second onset pressures for **3** are lower than those for **1**, and the adsorption maximum for **3** becomes lower than that for **1**. **4** has the coordinated DMF molecules at the Cu^{II} axial sites and coordination-free PF_6^- anions (shortest Cu···F distance = 5.9 Å).[11] Therefore, **4** is an ionic crystal. The adsorption isotherms of CO_2 for **4** reflect well the difference in the magnitude of the electrostatic interactions acting in the assembled structures. As shown in Figure 8, **4** shows no CO_2 adsorption up to a relative pressure of ~0.2 (point A). The CO_2 adsorption starts at point A, and **4** adsorbs one mole of CO_2 per mole of **4**. The onset relative pressure of **4**, at which structural transformation occurs, is considerably higher than those of **1** and **3**,

indicating that structural transformation in **4** is restricted by strong electrostatic interactions formed in the ionic crystal. Further structural transformation is not induced by an increase in pressure, because of a tight assembly in the ionic crystal. The IR spectra of **3** and **4** at 200 K under CO_2 flow support the formation of electron donor−acceptor interactions between the F atoms of the anions and CO_2 (see Figure S19 in the Supporting Information). Although the detailed assembled structure of **3** is unknown, it is worth noting that the exchange of axial ligands is a powerful method to regulate the adsorption property of CO_2. It should also be noted that the N_2 adsorption and desorption isotherms of **3** and **4** at 77 K (see Figure S12 in the Supporting Information) show a type II curve, indicative of no structural transformation to the porous form as well as **1**. As a result, we succeeded in tuning the CO_2 adsorption properties without a change in affinity for N_2 gas by modifying the axial ligands.

Conclusions

We have investigated the detailed CO_2 adsorption properties of the one-dimensional coordination polymer **1** with polar Cu−PF_6 parts. Originally, **1** has no pores to accommodate gas molecules. However, **1** shows a highly selective CO_2 adsorption behavior with three-step structural transformations. The results of the temperature-dependent IR spectra under CO_2 flow, calculations, and adsorption isotherms of CO_2 and C_2H_2, indicate that the specific adsorption sites may be on the surface of PF_6^- anions, which have the strongest polarity in the framework. The axial ligands of **1** (PF_6^- anions) are easily replaced by other anions (BF_4^-, **3**) or neutral ligands (DMF, **4**). Such treatments control the strength of polarity and, therefore, regulate the adsorption properties (onset pressures and amount adsorbed) for a specific targeted gas. These results pave the way for the development of high-performance separation materials for a specific guest.

Acknowledgment. We are grateful for financial support from ENEOS Hydrogen Trust Fund, Mukai Science and Technology Foundation, and Kumagai Foundation for Science and Technology. We wish to acknowledge Mr. H. Meguro (BEL Japan, Inc.) for the adsorption measurements of CO and H_2 gases. We thank Prof. M. Kato, Prof. H.-C. Chang, and Dr. A. Kobayashi (Hokkaido University) for allowing the use of their UV−vis reflection and temperature-dependent microscopic IR spectral apparatuses. We thank Ms. A. Tokumitsu and Ms. M. Kiuchi (Center for Instrument Analysis, Hokkaido University) for carrying out the elemental analysis.

Supporting Information Available: Complete list of authors for ref 16; synthetic procedure of $[CuCl_2(bpetha)]_n$ (**5**); UV−vis reflection spectra of **1** and **2**; ORTEP drawings of complexes I and II in **2** and α-$[Ni(NCS)_2(4\text{-mepy})_4]$ with the numbering scheme of the unique atoms; temperature dependence of solid-state ^{19}F-NMR spectra in **1** under the atmosphere; temperature dependence of the *g*-value and integrated intensity of ESR spectra in **1** under N_2 and CO_2 atmospheres; synchrotron XRD patterns of **1**; adsorption isotherms for CO_2, N_2, O_2, CO, and H_2 on **1** at 195 K; adsorption isotherms for Ar, CO, and H_2 on **1** at 77 K; solid-state MAS ^{19}F-NMR spectra (320 K) in KPF_6, $NaBF_4$, **1**·*n*H_2O, and **3**·*n*H_2O under the atmosphere; TG−DTA curves of **3** after exposure to acetone vapor; N_2 adsorption isotherms for **1**, **3**, and **4** at 77 K; XRD patterns of **3** and **4** after exposure to acetone vapor; the observed XRD pattern at 298 K and XRD pattern calculated from the single-crystal X-ray diffraction data of **4**; TG−DTA curves of **4**; XRD pattern and TG−DTA curves of **5**; adsorption isotherms for CO_2 on **5** at 195 K; IR spectra of **1**, **3**, **4**, and **5** under CO_2 flow at 200 K; molecular size and physical parameters of CO_2 and C_2H_2 (PDF and CIF). This material is available free of charge via the Internet at http://pubs.acs.org.